# Supplementary Materials: Mutated Human P-Selectin Glycoprotein Ligand-1 and Viral Protein-1 of Enterovirus 71 Interactions on Au Nanoplasmonic Substrate for Specific Recognition by Surface-Enhanced Raman Spectroscopy

**Kundan Sivashanmugan [1,2], Han Lee [1], Jiunn-Der Liao [1,3,*], Chen-Chu Wang [4], Chen-Hsueh Lin [1], Yuh-Shyong Yang [4] and Jaya Sitjar [1]**

1 Department of Materials Science and Engineering, National Cheng Kung University, Tainan 70101, Taiwan; sivashanmugannst87@gmail.com (K.S.); rick594007@hotmail.com (H.L.); az436436@gmail.com (C.-H.L.); jaya.sitjar@gmail.com (J.S.)
2 School of Electrical Engineering and Computer Science, Oregon State University, Corvallis, OR 97331, USA
3 Medical Device Innovation Center, National Cheng Kung University, 1 University Road, Tainan 70101, Taiwan
4 Department of Biological Science and Technology, National Chiao Tung University, Hsinchu 30010, Taiwan; rick594007@yahoo.com.tw (C.-C.W.); ysyang@faculty.nctu.edu.tw (Y.-S.Y.)
* Correspondence: jdliao@mail.ncku.edu.tw; Tel.: +886-6-2757575 (ext. 62971); Fax: +886-6-2346290

## 1. Experimental Section

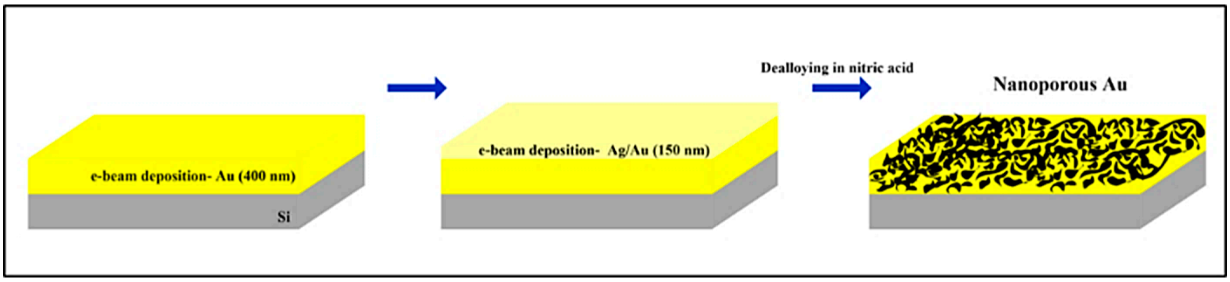


**Figure S1.** Schematic illustration of fabrication of Au nanoporous substrate.

## 2. Characterization of Au Nanoporous Substrate

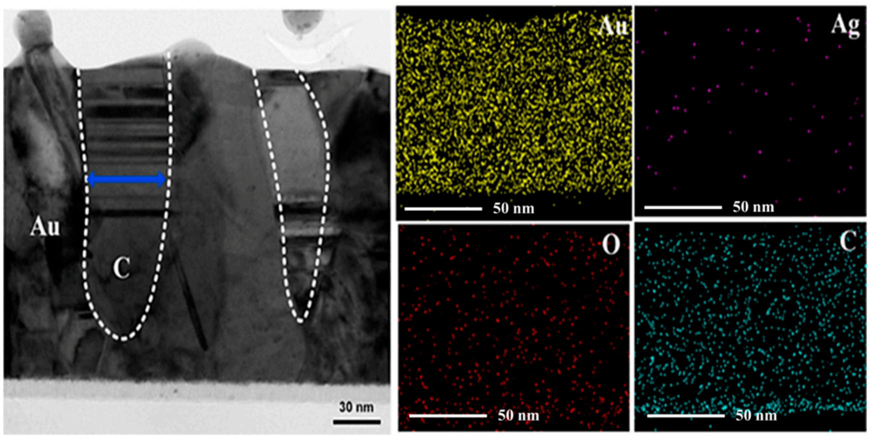


**Figure S2.** HR-FETEM image of optimized Au nanoporous substrate and EDS mappings of areas marked in HR-FETEM image.

**Table S1.** Nanopore size and contact angle of as-fabricated Au nanoporous substrates.

| Sample | Nanopore Size (±2 nm) | | Contact Angle (°) | |
|---|---|---|---|---|
| | 0.3 (Å/s) | 1 (Å/s) | 0.3 (Å/s) | 1 (Å/s) |
| Alloy | – | – | 80.23 | 80.23 |
| Aup_30s | 39 | 22 | 98.12 | 97.58 |
| Aup_60s | 46.5 | 41.3 | 76.08 | 75.88 |
| Aup_90s | 50 | 44.7 | 76.00 | 75.13 |
| Aup_120s | 60.7 | 50.7 | 75.61 | 74.65 |
| Aup_150s | 66.6 | 57 | 75.43 | 74.41 |
| Aup-180s | 73.7 | 61.8 | 75.27 | 74.19 |
| Aup_210s | 85.8 | 66.3 | 75.15 | 74.5 |

3. **Optical Properties of Au Nanoporous Substrate**

The COMSOL calculated Au nanoporous cavity width and length were 60 and 90 nm, respectively, with and without roughness of surface. Figure S(3c) shows the simulation results of the SPR shift and local field distributions on the Au nanoporous cavity surface. The strong SPR peaks obtained at 605 nm calculated for the nanoporous substrate are due to high plasmonic coupling generated in the porous cavity environment. In addition, the EF increased with increasing roughness of porous cavities.

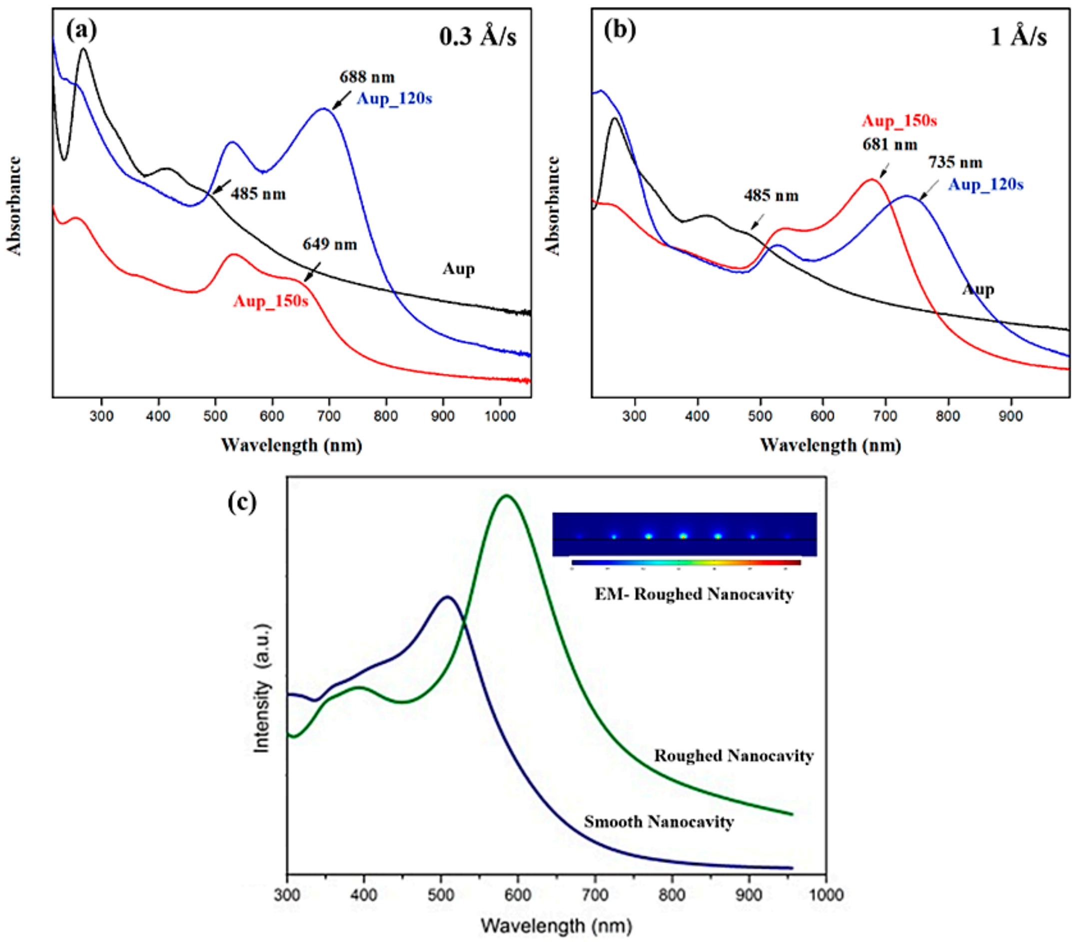


**Figure S3.** SPR spectra of as-fabricated Au nanoporous substrate created at deposition rates of (**a**) 0.3 Å/s and (**b**) 1 Å/s with optimized dealloying times (120 and 150 s, respectively). (**c**) COMSOL calculation of smooth and roughed Au nanocavity.

## 4. SERS Characterization of PPIs on Au Nanoporous Substrate

**Table S2.** Raman assignment for protein immobilized on Au nanoporous substrate [1–12].

| 3APTES | 3APTES + Glu | GST-PSGL-1 | S-GST-PSGL-1 | Raman Assignment |
|---|---|---|---|---|
| 629, 677 | 670 | 671 | 647 | ʋ(C–C), ʋ(C–S), amino acid (tyrosine) |
| 751 | 784 | 778, 742 | 694, 753 | ʋ(C–S) |
| 813 | – | – | 805 | (C–O–C) weak |
| – | – | 827 | 851 | $NH_2$, $CH_2$ wag |
| 861 | 878 | – | 873, 888 | ϱ$CH_2$, δ$CH_3$ |
| 948 | 903 | 974 | 950 | $CH_2$, Carboxylic acid |
| – | – | – | 984 | $SO_4^{2-}$ |
| 1007 | 1005 | – | – | Si–O–Si, Si–O–C |
| – | – | – | 1030 | $-SO_3$ |
| – | 1046 | 1035 | | $C_4N^+$ stretching |
| – | – | – | 1077 | C–C in-plane bending, $-SO_3$ |
| 1101 | 1113, 1162 | 1132, 1172 | 1121, 1150 | ʋ(C=S), (C–C) stretching, $CH_3$, $CH_2$ twisting, $-SO_3$ |
| 1188 | – | – | 1192 | $-SO_3$ |
| 1240 | 1206 | 1222 | 1237 | C–C stretching, CO in ring stretching CH of ring, Amide III |
| 1288 | – | 1261 | – | C–C stretching, C–N Stretching, S=O |
| 1312 | – | 1304 | – | δ($CH_2$) twisting or wagging of protein |
| 1336 | 1326 | 1348 | 1325, 1345 | Nitro, Amide III, and $CH_2$ wagging vibrations from glycine backbone |
| 1379 | – | – | 1380 | C–$CH_3$, δ$CH_3$ symmetric (lipid assignment) |
| 1486 | 1438 | 1419, 1449, 1498 | 1409, 1451, 1477 | $CH_2$/$CH_3$ deformation of lipids and proteins |
| 1534 | 1501, 1528 | – | 1530, 1548, 1572 | C–N, Nitro, Amide |
| – | – | 1584 | 1589 | C=C aromatic |
| 1601 | 1593, 1657 | 1619 | 1627 | O–C=O stretching |

**Table S3.** Raman assignment for protein mutants on Au nanoporous substrate [1–12].

| M0 | M1 | M2 | M3 | M4 | M5 | M6 | M7 | Raman Assignment |
|---|---|---|---|---|---|---|---|---|
| 647, 693, 752 | 674 | 729 | – | 622, 794 | 778 | 637, 677, 771 | 621, 689, 728 | ʋ(C–C), ʋ(C–S), amino acid |
| 824 | 812 | – | – | – | – | – | – | $NH_2$, $CH_2$ wag |
| 870 | – | – | – | – | 886 | – | 891 | ϱ$CH_2$, δ$CH_3$ |
| 950 | – | – | – | – | – | 949 | 914 | $CH_2$, carboxylic acid |
| 986 | – | 982 | – | – | – | – | – | $SO_4^{2-}$ |
| – | 1004 | 1002 | 999 | 998 | 999 | 998 | 1001 | Phenylalanine |
| 1030 | – | – | – | – | – | – | – | $-SO_3$ |
| 1084 | – | – | – | – | – | 1067 | 1082 | $C_4N^+$ stretching, $-SO_3$ |
| 1122, 1151, 1194 | | 1148 | 1148 | | 1118, 1148 | 1124 | 1103, 1166 | $-SO_3$ |
| 1239 | 1216 | 1270 | – | 1261 | 1278 | – | 1261 | S=O |
| – | – | – | – | – | – | – | 1302 | δ($CH_2$) twisting or |

| | | | | | | | | |
|---|---|---|---|---|---|---|---|---|
| | | | | | | | | wagging of protein |
| 1323 | – | – | – | – | 1328 | – | 1326, 1347 | Nitro, amide III, and $CH_2$ wagging vibrations from glycine backbone |
| – | 1361 | 1387 | 1390 | 1385 | 1397 | 1388 | – | C–$CH_3$, δ$CH_3$ symmetric (lipid assignment) |
| 1412, 1449 | 1452 | – | – | – | 1452, 1496 | 1475 | 1410, 1499 | $CH_2$/$CH_3$ deformation of lipids and proteins |
| 1532, 1548, 1574 | 1531, 1576 | 1570 | – | 1515 | 1536, 1554 | 1510, 1543, 1570 | 1552 | C–N, nitro, amide |
| – | – | – | | 1585 | – | – | – | C=C aromatic |
| 1591, 1626 | 1638 | 1622, 1649 | 1595, 1622 | 1626 | 1602, 1632 | 1592, 1631 | 1644 | O–C=O stretching |

Samples are denoted as M0 (46, 48, 51), M1 (46F), M2 (48F), M3 (51F), M4 (46F, 48F), M5 (46F, 51F), M6 (48F, 51F), and M7 (46F, 48F, 51F).

**Table S4.** Raman assignment for protein-antibody interaction on Au nanoporous substrate [1–13].

| Anti-Sulfotyrosine | S-GST-PSGL-1 | Raman Assignment |
|---|---|---|
| 649, 789 | 659, 743, 799 | υ(C–S) |
| 888 | 840, 878 | ϱ$CH_2$, δ$CH_3$, $NH_2$ |
| – | 901 | $CH_2$, carboxylic acid |
| 989 | 978 | $SO_4^{2-}$ |
| 1025 | – | –$SO_3$ |
| 1057 | 1057 | $C_4N^+$ stretching |
| 1112,1135 | 1115,1194 | –$SO_3$ |
| 1248, 1285 | 1223, 1282 | –$SO_3$, S=O |
| 1333, 1377 | 1338, 1396 | Nitro, amide III, $CH_2$ wagging, δ$CH_3$ symmetric (lipid assignment) |
| 1401, 1452,1483 | 1449 | $CH_2$/$CH_3$ deformation of lipids and proteins |
| 1534 | 1531, 1556 | C–N, nitro, amide |
| – | 1597 | C=C aromatic |
| 1642, 1684 | 1701,1764,1801 | H–C=O, O–C=O stretching |

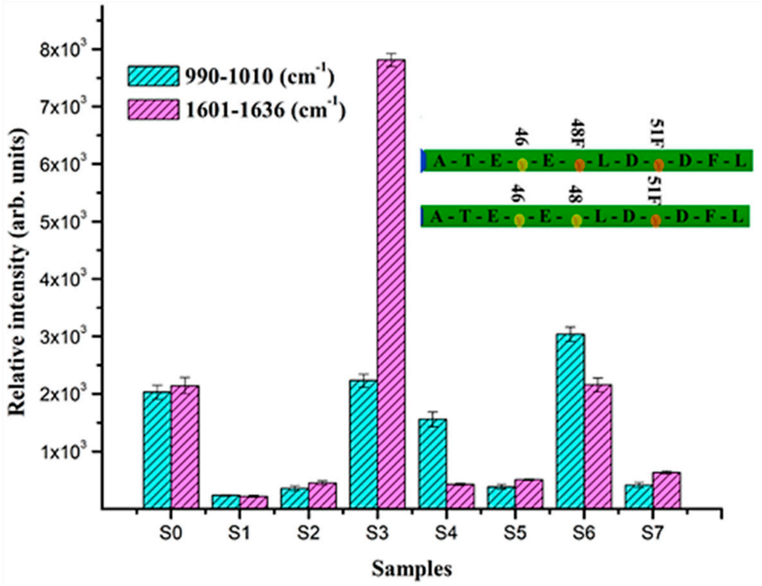


**Figure S4.** Relationship of relative Raman intensities for various mutants and antibody-sulfotyrosine interactions on Au nanoporous substrate determined using $I_{SERS}$ peak regions at 990–1010 and 1601–1636 cm$^{-1}$.

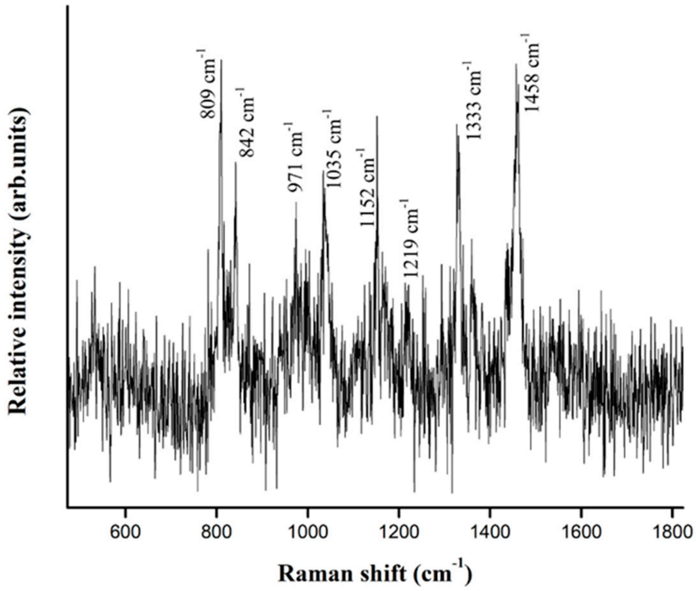


**Figure S5.** VP1 of EV71 on Au nanoporous substrate examined at Raman laser wavelength of 633 nm.

**Table 5.** Raman assignment for PPIs on Au nanoporous substrate [3–13].

| V0 | V1 | V2 | V3 | V4 | V5 | V6 | V7 | Raman Assignment |
|---|---|---|---|---|---|---|---|---|
| 652 | 665 | 675 | 629, 757 | 648, 681, 793 | 659 | 645, 676 | 708 | ʋ(C–C), ʋ(C–S), amino acid |
| – | 813 | 826 | 822 | – | – | 838 | – | $NH_2$, $CH_2$ wag |
| – | – | 886 | 886 | 870 | – | 858 | 882 | ϱ$CH_2$, δ$CH_3$ |
| – | – | 948 | | 931 | 954 | – | | $CH_2$, carboxylic acid |
| – | – | – | 983 | – | – | – | 978 | $SO_4^{2-}$ |
| 1014 | – | 993 | – | – | – | – | | Phenylalanine |
| | – | 1028 | – | 1036 | – | – | 1028 | –$SO_3$, phenylalanine |
| 1099 | – | 1070 | – | 1087 | – | 1078 | – | $C_4N^+$ stretching, –$SO_3$ |

| | | | | | | | | |
|---|---|---|---|---|---|---|---|---|
| – | 1121 | 1114, 1154 | 1168 | 1105, 1139, 1183 | – | 1158, 1174 | 1131 | $-SO_3$ |
| 1237 | 1262 | 1215, 1240, 1288, | 1239 | 1219 | – | 1254 | 1248 | S=O |
| – | – | – | 1316 | – | – | 1329 | – | Nitro, amide III, and $CH_2$ wagging vibrations from glycine backbone |
| 1361 | – | 1349 | – | 1353, 1391 | 1350 | – | 1370 | C–$CH_3$, δ$CH_3$ symmetric (lipid assignment) |
| 1407, 1489 | – | 1425, 1495 | 1402 | 1451 | – | 1420, 1454, 1495 | 1474 | $CH_2$/$CH_3$ deformation of lipids and proteins (tyrosine) |
| 1531, 1555 | 1520, 1535 | 1562 | 1532 | 1543 | 1550, 1567 | 1523, 1550, 1579 | 1531, 1574 | C–N, nitro, amide |
| 1592 | – | – | 1580, | 1589 | – | – | – | C=C aromatic |
| 1600, 1618 | 1600 | 1601, 1621 | 1601, 1628 | 1600, 1614, 1643 | 1600, 1633 | 1602, 1644 | 1600, 1618 | O–C=O stretching |

Samples are denoted as V0 (46, 48, 51), V1 (46F), V2 (48F), V3 (51F), V4 (46F, 48F), V5 (46F, 51F), V6 (48F, 51F), and V7 (46F, 48F, 51F).

## References


1. Fischer, W.B.; Eysel, H.H. Polarized Raman spectra and intensities of aromatic amino acids phenylalanine, tyrosine and tryptophan. *Spectrochim. Acta A: Mol. Spectrosc.* **1992**, *48*, 725–732.
2. Ashton, L.; Brewster, V.L.; Correa, E.; Goodacre, R. Detection of glycosylation and iron-binding protein modifications using Raman spectroscopy. *Analyst* **2017**, *142*, 808–814.
3. Li, Y.T.; Li, D.W.; Cao, Y.; Long, Y.T. Label-free in-situ monitoring of protein tyrosine nitration in blood by surface-enhanced Raman spectroscopy. *Biosens. Bioelectron.* **2015**, *69*, 1–7.
4. Ravikumar, B.; Rajaram, R.K.; Ramakrishnan, V. Raman and IR spectral studies of L-phenylalanine L-phenylalaninium dihydrogenphosphate and DL-phenylalaninium dihydrogenphosphate. *J. Raman Spectrosc.* **2006**, *37*, 597–605.
5. Singho, N.D.; Johan, M.R. Complex impedance spectroscopy study of silica nanoparticles via sol-gel method. *Int. J. Spectrosc.* **2012**, *2012*, 7.
6. Brewster, V.L.; Ashton, L.; Goodacre, R. Monitoring the glycosylation status of proteins using Raman spectroscopy. *Anal. Chem.* **2011**, *83*, 6074–6081.
7. Davies, H.S.; Singh, P.; Deckert-Gaudig, T.; Deckert, V.; Rousseau, K.; Ridley, C.E.; Dowd, S.E.; Doig, A.J.; Pudney, P.D.A.; Thornton, D.J.; et al. Secondary structure and glycosylation of mucus glycoproteins by Raman spectroscopies. *Anal. Chem.* **2016**, *88*, 11609–11615.
8. Madzharova, F.; Heiner, Z.; Kneipp, J. Surface enhanced hyper-Raman scattering of the amino acids tryptophan, Histidine, Phenylalanine, and Tyrosine. *J. Phys. Chem. C* **2017**, *121*, 1235–1242.
9. Arp, Z.; Autrey, D.; Laane, J.; Overman, S.A.; Thomas, G.J. Tyrosine Raman signatures of the filamentous virus Ff are diagnostic of non-hydrogen-bonded phenoxyls: demonstration by Raman and infrared spectroscopy of p-cresol vapor. *Biochemistry* **2001**, *40*, 2522–2529.
10. Hernández, B.; Pflüger, F.; Kruglik, S.G.; Ghomi, M. Characteristic Raman lines of phenylalanine analyzed by a multiconformational approach. *J. Raman Spectrosc.* **2013**, *44*, 827–833.
11. Li, X.; Martin, S.J.H.; Chinoy, Z.S.; Liu, L.; Rittgers, B.; Dluhy, R.A.; Boons, G.-J. Fast production of self-assembled hierarchical $\alpha$-$Fe_2O_3$ nanoarchitectures. *Chem.A Eur. J.* **2016**, *22*, 11180–11185.

12. Lu, X.; Liu, Q.; Benavides-Montano, J.A.; Nicola, A.V.; Aston, D.E.; Rasco, B.A.; Aguilar, H.C. Detection of receptor-induced glycoprotein conformational changes on enveloped virions by using confocal micro-Raman spectroscopy. *J. Virol.* **2013**, *87*, 3130–3142.
13. Sivashanmugan, K.; Liu, P.-C.; Tsai, K.-W.; Chou, Y.-N.; Lin, C.-H.; Chang Y.; Wen, T.-C. An anti-fouling nanoplasmonic SERS substrate for trapping and releasing a cationic fluorescent tag from human blood solution. *Nanoscale* **2017**, *9*, 2865–2874.